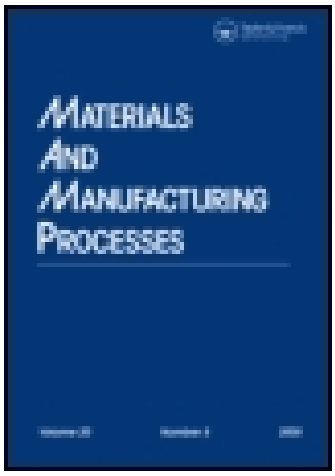

Materials and Manufacturing Processes
Publication details, including instructions for authors and subscription information:
http://www.tandfonline.com/loi/lmmp20

An Investigation of Friction During Friction Stir Welding of Metallic Materials

K. Kumar [a], C. Kalyan [b], Satish V. Kailas [a] & T. S. Srivatsan [c]
[a] Department of Mechanical Engineering, Indian Institute of Science, Bangalore, India
[b] Department of Metallurgy, College of Engineering, Salem, Tamil Nadu, India
[c] Department of Mechanical Engineering, The University of Akron, Akron, Ohio, USA
Published online: 26 Feb 2009.

To cite this article: K. Kumar, C. Kalyan, Satish V. Kailas & T. S. Srivatsan (2009) An Investigation of Friction During Friction Stir Welding of Metallic Materials, Materials and Manufacturing Processes, 24:4, 438-445, DOI: 10.1080/10426910802714340

To link to this article: http://dx.doi.org/10.1080/10426910802714340

Materials and Manufacturing Processes, 24: 438–445, 2009

ISSN: 1042-6914 print/1532-2475 online
DOI: 10.1080/10426910802714340

Taylor & Francis
Taylor & Francis Group

An Investigation of Friction During Friction Stir Welding of Metallic Materials

K. Kumar[1], C. Kalyan[2], Satish V. Kailas,[1] and T. S. Srivatsan[3]

[1]*Department of Mechanical Engineering, Indian Institute of Science, Bangalore, India*
[2]*Department of Metallurgy, College of Engineering, Salem, Tamil Nadu, India*
[3]*Department of Mechanical Engineering, The University of Akron, Akron, Ohio, USA*

The technique of friction stir welding (FSW) puts effective use frictional heat for the purpose of joining metallic materials. In this research article, we present and discuss an experimental method to determine the coefficient of friction during FSW. The experiments were conducted to study the interaction between the FSW tool (a die steel) and the base metal (a high strength aluminum alloy) at various contact pressures (13 MPa, 26 MPa, and 39 MPa) and rotation speeds (200 rpm, 600 rpm, 1000 rpm, and 1400 rpm). The experimental results, the microstructure, and the process temperature reveal the experimental setup to be capable of simulating the conditions during FSW. The coefficient of friction was found to vary from 0.15 to 1.4, and the temperature increased to as high as 450°C. The coefficient of friction was found to increase with temperature. There exists a critical temperature at which point a steep increase in the coefficient of friction was observed. The critical temperature decreases from 250°C at a contact pressure of 26 MPa to 200°C at contact pressure of 34 MPa. Below the critical temperature at a specific contact pressure the maximum coefficient of friction is 0.6, and above the critical temperature it reaches a value as high as 1.4. The steep increase in the coefficient of friction is found to be due to the seizure phenomenon and the contact condition during FSW between the tool and the workpiece (base metal) is found to be sticking.

Keywords Aluminum alloys; Coefficient of friction; Contact condition; Friction stir welding; Heat generation; Microstructure; Sticking/Slipping.

1. Introduction

The technique of friction stir welding, referred to henceforth throughout this article as FSW, was invented at The Welding Institute (TWI), United Kingdom in the early 1990s and was initially tried on aluminum alloys [1, 2]. The FSW technique did prove itself ideal for creating good quality butt joints and lap joints [3–6] in a number of materials, especially the family of nonferrous metallic materials to include even those that are extremely difficult to weld by conventional fusion welding processes [7]. During FSW, the frictional heat that is generated is effectively utilized to facilitate material consolidation and eventual joining with the aid of an axial pressure. The process is shown in Fig. 1. In this technique, a nonconsumable rotating tool having a specially designed pin, also known as probe, and having a shoulder, is referred to as the FSW tool. The tool is inserted into the abutting edges of the material to be joined until the shoulder is in direct contact with the two pieces of plates or sheets that are to be butt-welded. The tool is then progressively traversed along the line of the weld using a normal load.

The pin initially makes contact as it is plunged into the joint region. The friction arising from the initial plunging heats up a cylindrical column of metal immediately around the pin as also a small region of the metal immediately below the pin. The localized heating arising from friction between the rotating tool and the static workpiece promotes localized microplastic deformation of the workpiece. The highly localized and concentrated heating aids in softening of the material that is both around and adjacent to the pin. This coupled with a combination of tool rotation and a gradual translation of the tool through the material to be joined facilitates in a movement of metallic material from the front of the rotating pin to the rear of the rotating pin. The process results in the production of a joint that is produced in the solid state.

The depth of penetration into the material being joined is controlled by length of the pin below the shoulder of the tool. The shoulder, which is in direct contact with the material to be joined, applies additional frictional heat to the weld region while concurrently aiding in preventing the highly plastic material from being expelled during the welding operation. The softened region of the material due to the generation of friction heat is wider at the top surface that is in direct contact with the shoulder of the tool and gradually tapers down to the pin diameter. The combined friction heat from the rotating pin and the shoulder of the tool creates a near plastic condition (i) immediately around the immersed pin, and (ii) at the contact surface of the shoulder with the top surface of the workpiece. The material gradually flows around the rotating tool and coalesces behind the tool as relative movement of the rotating tool on the substrate (workpiece) takes place. The noticeable advantages of this technique are the following:

(i) The consolidated welds are solid phase and reveal no evidence of fusion welding defects;
(ii) No consumable filler material, shielding gas, or edge preparation is normally used to get the final weld;

Received November 28, 2008; Accepted August 8, 2008
Address correspondence to Satish V. Kailas, Department of Mechanical Engineering, Indian Institute of Science, Bangalore 560 012, India; E-mail: satvk@mecheng.iisc.ernet.in

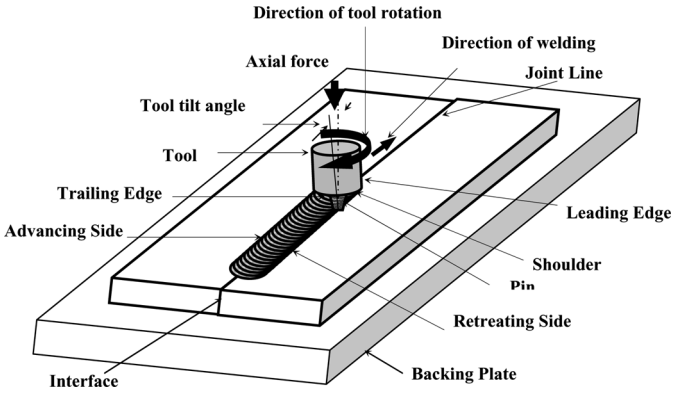

FIGURE 1.—Schematic diagram explaining the FSW process.

(iii) The distortion of the workpiece is noticeably less than that caused by the traditional fusion welding techniques.

A simultaneous rotation and translation motion of the tool during the welding process creates a characteristic asymmetry between the adjoining sides. Where the tool rotation is in the same direction as translation of the welding tool, the side is referred to as the advancing side (AS). On the other side, when the rotation of the tool and translation motion of the tool counteract with each other, this is referred to as the retreating side (RS).

The temperature during a typical FSW process is found to be in the range of 450–480°C [8] for the welding of aluminum, and the pressure reported was equivalent to the yield pressure [9] of the material at the temperature.

The two most important parameters that must be controlled in the forming of sound welds are the heat input and material flow. The coefficient of friction does have an influence on frictional heat generation, while the interface condition has an effect on the material flow characteristics [8]. Further, the thermal models that aim at an accurate prediction of the temperature during the FSW process require precise frictional data. Despite the prevailing discrepancy between the theoretical value and experimental value of the friction coefficient, in thermal modeling of the FSW technique the coefficient of friction (μ) is assumed to be 0.4 for purpose of calculations at various temperatures and pressures [9–12]. Similarly, Schmidt and Huttel [13] reported that the coefficient of friction is assumed in many cases instead of actual measurement. However, for purpose of a realistic model there exists a need for experimental frictional data. Colligan and Mishra [14] reported in their research publication the lack of a detailed study on the variation of friction coefficient, particularly at the temperatures and relative velocities commonly experienced during FSW. Hence, it is important to study and concurrently document the frictional characteristics of the rotating tool with the base-metal for purposes of enhancing our understanding of the heat input characteristics during FSW.

The existence, nature, and severity of friction between the similar and dissimilar pairs of several materials (metals) have been analyzed particularly for sliding conditions at different temperatures and contact pressure. However, the frictional characteristics that exist at high temperatures and pressures are still not very well understood [15]. Thomson and Chen [16] rationalized, using a theoretical approach, that the coefficient of friction cannot be greater than 0.577. Around the same time Duffin and Bahrani [17] experimentally determined the friction coefficient to exceed 0.57 during friction welding, and they reported the coefficient of friction to be 1.5, 1.9, 2.1, and 2.7 for the welding of mild steel. Similar results were reported by Reid and Schey [18] for the welding of pure copper. However, none of the existing theories can convincingly explain the phenomenon of friction that exists, prevails, and exerts an influence during FSW.

An important item to be noted in the FSW experiments is that the experimental setup(s) are designed to simulate the actual working conditions. This is due to the fact that the frictional behavior is highly sensitive to the working environment. Schmidt and Huttel [13] explained the requirement for an enormous experimental setup and the complexity involved in measuring the coefficient of friction, under strain-rate in terms of $1000\,s^{-1}$, for a temperature range between room temperature (25°C) and solidus temperature of the metal being tested. Thus, in order to generate the FSW condition in the experimental setup and to experimentally evaluate the coefficient of friction, proposed by Schmidt and Huttel [13], the only way is to use the process itself. Since the instrumented FSW machines are very expensive, it is not an economically affordable and viable technique. Hence, there does exist a need for the development of a simple experimental procedure, which can clearly simulate the conditions that exist during FSW.

In this independent research article, we provide a brief overview of an innovative inexpensive experimental technique that was developed, wherein the FSW condition is simulated, and the value of the coefficient of friction is experimentally found for aluminum alloy (7020-T6) base metal and a hot die steel (Grade: H13) tool for various values of the tool rotational speed, contact pressure, and temperature.

2. EXPERIMENTAL DETAILS

The materials chosen for this experimental study were a hot die steel (Grade: H13) and an aluminum alloy (7020-T6). The hot worked die steel is a common tool material that is chosen for the welding of aluminum alloys. Alloy 7020-T6 is a ternary (Al–Zn–Mg) precipitation hardened aluminum alloy, which is often chosen and used as a structural material primarily in the industry of aerospace and to a limited extent in the automobile industry. This alloy gains its strength form the complex precipitation of Guinier–Preston (GP) zones and the η' (semi-coherent $MgZn_2$) phase in the microstructure. This is achieved by solution treatment and controlled aging of the ternary alloy. The GP zones and η' phases are stable in the temperature range of 20–120°C and 120–250°C, respectively [19, 20]. Above the stable temperature range the equilibrium η phase (noncoherent $MgZn_2$) is precipitated through the matrix resulting from a transformation of the existing η' phase. Formation and presence of the η phase in the

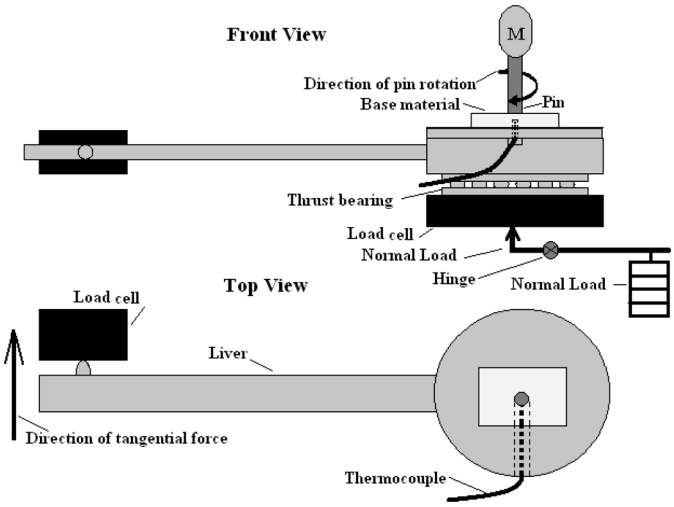

FIGURE 2.—The schematic diagram showing the experimental setup.

microstructure reduces the material strength, and this is known as *overaging*.

The experimental setup is schematically shown in Fig. 2. In this setup, the cylindrical pin is carefully rotated around its axis using a motor. The base metal is either fixed or held on to the lever assembly, which is kept on a thrust bearing. The rotating pin of diameter 7 mm and the surface of a 4.4 mm thick aluminum alloy sheet are brought into direct contact with each other using a predefined normal load, which applies an average contact pressure of 13 MPa, 26 MPa, and 39 MPa on the surface of the base metal. A normal load is applied from the bottom through a load cell and using a fulcrum. The tangential load on the aluminum alloy sheet is measured using a load cell that was positioned at a distance of 150 mm from the axis of the rotating pin.

During the experiments the tangential force was continuously collected through a data logger. The experiments were conducted for a combination of three different axial loads and four different rotation speeds. The test parameters used are summarized in Table 1. Apart from the axial load and rotation speed, the rise in temperature that occurs due to frictional heating is used to study the intrinsic influence of temperature. The process temperature was measured using a K-type thermocouple that was positioned on the base metal up until the mid-plane. The temperature readings were manually recorded at periodic intervals of 30 seconds.

TABLE 1.—Combinations of axial load and the rotation speeds used.

Sl. No	Axial load (N)	Rotation speed (rpm)
1	500	200
2	500	600
3	500	1000
4	500	1400
5	1000	200
6	1000	600
7	1000	1000
8	1000	1400
9	1500	200
10	1500	600
11	1500	1000
12	1500	1400

The average coefficient of friction values was calculated from the measured tangential load and applied axial load. Details of the calculations are provided in the following section. After the experiments, the microstructure of the subsurface of the aluminum alloy specimens was examined by cutting the specimens perpendicular to the surface along the diameter of the interaction area. The cut samples were prepared for micrographic examination using standard metallographic procedures. The mechanically ground and fine polished specimens were then etched using Keller's reagent (a solution mixture of nitric acid + hydrofluoric acid and distilled water). The microstructure of the subsurface was observed in an optical microscope and photographed using the bright field illumination technique.

3. CALCULATION OF THE FRICTION COEFFICIENT

The coefficient of friction is calculated from the measured tangential force at a distance away from axis of the pin. The torque generated by the rotating pin is given by the expression

$$T = 1/12\pi\mu PD^3. \tag{1}$$

In this equation, P is contact pressure, and D $(=2R)$ is diameter of the rotating pin. The average contact pressure is given by the expression

$$P = \frac{4N}{\pi D^2}. \tag{2}$$

In this expression, N is the normal force.

Substituting Eq. (2) into Eq. (1), we get

$$T = 1/3\mu DN. \tag{3}$$

Simplifying this equation to obtain the coefficient of friction, we get

$$\mu = \frac{3T}{DN}. \tag{4}$$

In the experimental setup used in this study, the tangential force was measured using a load cell that was positioned at a distance of 150 mm from the axis of the rotating pin. Hence, the coefficient of friction is

$$\mu = \frac{450L}{DN}, \tag{5}$$

where L is the tangential load measured by the load cell that is located at a distance of 150 mm away from the axis of the pin.

4. RESULTS AND DISCUSSION

4.1. Coefficient of Friction and Temperature

The variation of coefficient of friction with sliding time is established for different rotation speeds for average contact

pressures of 13 MPa, 26 MPa, and 39 MPa. Variation of the corresponding rise in temperature with time is shown in Figs. 3(b) to 5(b).

4.1.1. Contact Pressure of 13 MPa. For the set of experiments conducted at an average contact pressure of 13 MPa, the coefficient of friction is between 0.15 and 0.4 for all chosen rotation speeds. Further, with time, the coefficient of friction initially decreases and then abruptly increases during the later stages of the experiment particularly at rotation speeds of 600 rpm and 1000 rpm. As reported by Farhat and coworker [21], during the initial stages of interaction between the rotating tool and the workpiece surface the frictional properties are governed by the fresh base metal grains that are continuously exposed. As the interaction progresses both the surface and the material in the subsurface deform, and the hardness increases due to the intrinsic influence of strain hardening. During the later stages the frictional properties are governed not by properties of the fresh metal but by properties of the strain hardened material, which is essentially harder than the initial metal. This phenomenon reduces the coefficient of friction gradually until an interaction of "local" debris that is generated with the interacting surfaces, as shown in Fig. 3(a).

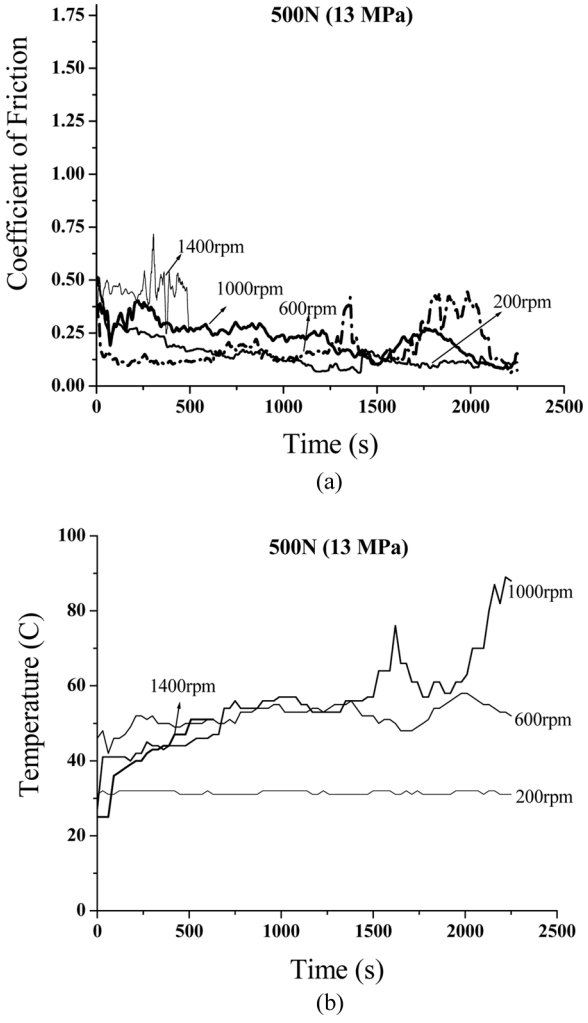

FIGURE 3.—(a) Coefficient of friction as a function of time (seconds) and (b) Process temperature as a function of time (seconds) at contact pressure of 13 MPa.

In the experiments conducted at a contact pressure of 13 MPa and rotational speeds of 200 rpm and 600 rpm the temperature rise is not appreciable and reaches a steady state. For the experiment conducted at a rotation speed of 1000 rpm, the temperature rises up to 80°C but there is a minimal effect on the coefficient of friction. The experiments conducted at rotation speed of 1400 rpm the contact pressure causes a vibration of the experimental setup arising from severe wear coupled with the formation of wear debris of aluminum. This caused the experiment to stop after a short duration of time. The volume of wear debris that formed at constant pressure is proportional to the sliding distance when there exists no appreciable rise in temperature at the interface. The observed increase in the coefficient of friction during the later stages of the experiments at rotation speeds of 600 rpm and 1000 rpm can be attributed to the formation of wear debris coupled with an interaction of debris with the interface. In the current experimental setup, there is no provision for the debris to be expelled from the interacting surfaces. Consequently, the debris ends up interacting with the interacting surfaces. Also, the interacting surfaces are not exposed to the atmosphere following the initial contact, since the rotating die steel pin is interacting with the static aluminum alloy plate at the same place. The vibration that occurs at the rotation speed of 1400 rpm could be caused by the formation and presence of wear debris in the "bulk." This analogy was utilized for the condition monitoring of machines by Peng and coworkers [22] based on vibration analysis that occurs due to the formation of the debris.

4.1.2. Contact Pressure of 26 MPa. In the set of experiments conducted at an average contact pressure of 26 MPa, the coefficient of friction is between 0.2 and 0.4 during the initial stages of the experiment and for all rotational speeds, as shown in Fig. 4(a). In this set of experiments, the temperature is higher at the higher rotation speeds due to higher power input. The steady state coefficient of friction is observed to be the following:

(a) 0.2 when the temperature is below 50°C;
(b) 0.4 when the temperature is between 100 and 200°C;
(c) 1.2 when the temperature is 400°C.

At the rotation speed of 200 rpm the trend shown by the friction and the resultant temperature increase are quite similar to the one seen at a contact pressure of 13 MPa. At rotation speeds of 600 rpm, 1000 rpm, and 1400 rpm, during the initial stages the coefficient of friction increases from the starting value.

(i) At rotation speed of 600 rpm, the coefficient of friction increases from 0.25 to 0.6, and then decreases to 0.12. At this rotation speed, the temperature follows a similar trend. The formation of debris during the initial stages of the experiment causes an initial increase in

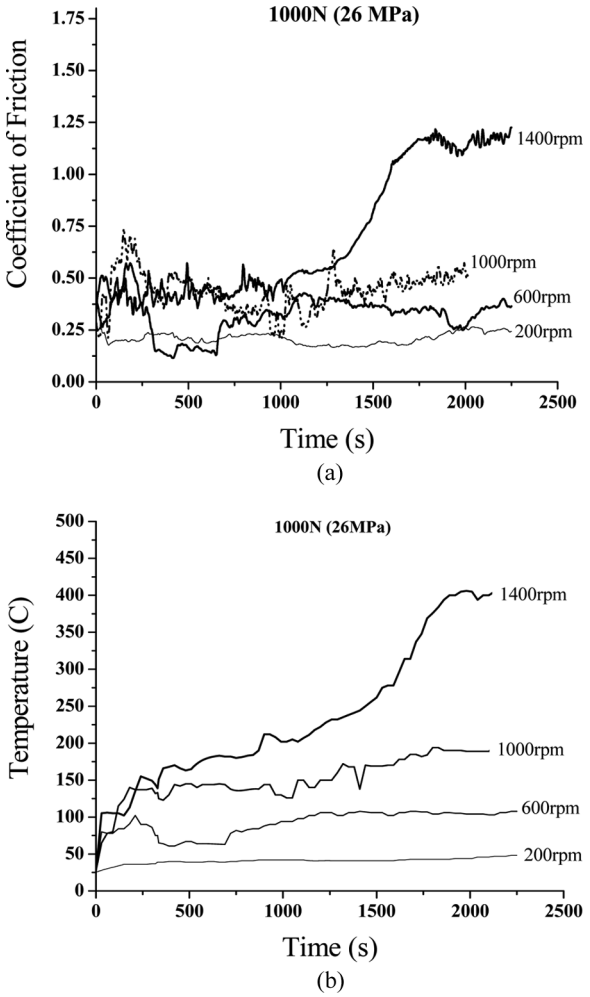

FIGURE 4.—(a) Coefficient of friction with time (seconds) and (b) Process temperature as a function of time (seconds) at contact pressure of 26 MPa.

the coefficient of friction, which is observed in all the experiments. Consequently, an interaction of the rotating tool with the work hardened base metal reduces the friction coefficient. The decreased value of the coefficient of friction is equal to the one seen for the experiments conducted at contact pressure of 13 MPa and for rotational speeds of 200 rpm, 600 rpm and 1000 rpm. As time progresses, the coefficient of friction increases to 0.4, and a steady state is reached. This is attributed to a "local" softening of the material that occurs due to dissolution of the GP zones in the temperature range of 100°C.

(ii) At rotational speed of 1000 rpm, after an initial peek, there is slight decrease in the coefficient of friction before becoming steady thereafter. However, there is no observed reduction in the friction coefficient to 0.16 as seen for the rotation speed of 600 rpm. The steady state temperature for rotation speed of 1000 rpm was observed to be 150°C and increases only slightly during the later stages. The coefficient of friction observed in this region is equal to the one observed for rotational speed of 600 rpm, where the material is expected to be locally softer due to a dissolution of the GP zones.

(iii) The experiment conducted at rotation speed of 1400 rpm the coefficient of friction increases initially from 0.25 to 0.4 and remains at 0.4 for some time before rising steeply to 1.2. This transition was clearly noticed when temperature at the "local" level rises above 120°C and 250°C. The coefficient of friction was found to be 0.4 up until 250°C. When the temperature increases beyond 250°C, the coefficient of friction increases steeply to 1.2 [Fig. 4(a)]. A similar trend is observed with temperature, and it increases gradually up until 250°C, and rapidly thereafter to 400°C.

4.1.3. Contact Pressure of 39 MPa. The results of experiments conducted at a contact pressure of 39 MPa are presented in Fig. 5. The coefficient of friction in the experiment conducted at rotation speed of 200 rpm is around 0.2 during the initial stages and decreases to 0.12 during the later stages. The temperature does not increase above 50°C.

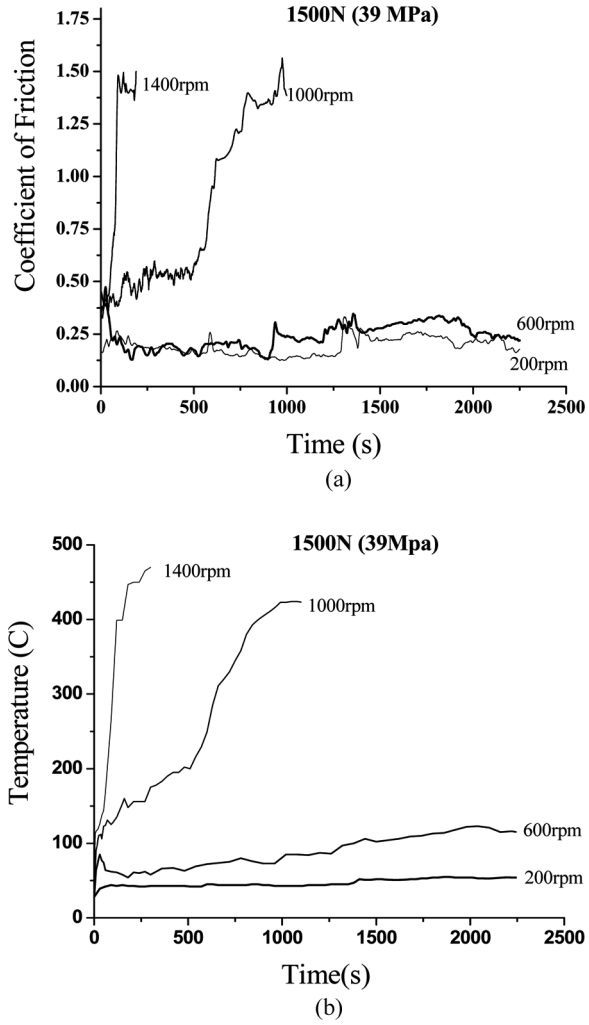

FIGURE 5.—(a) Coefficient of friction with time (seconds) and (b) Process temperature as a function of time (seconds) at contact pressure of 39 MPa.

(i) At the rotation speed of 600 rpm, the coefficient of friction initially increased from 0.3 to 0.4 and then decreases to 0.12 until the temperature increases up to 100°C. When the temperature reaches 100°C, the coefficient of friction increases to 0.25. The increase in coefficient of friction is not as high as was seen for the contact pressure of 26 MPa at the rotation speed of 600 rpm.

(ii) At the rotation speed of 1000 rpm, the coefficient of friction is around 0.3 and gradually increases to 0.6 at an axial load of 39 MPa till the process temperature reaches 200°C. Beyond this temperature, the increase in the coefficient of friction is steep from 0.6 to 1.4.

The experimental results reveal the temperature of the base material to have a remarkable influence on the coefficient of friction, which can be easily associated with intrinsic metallurgical changes experienced by the base metal. It is observed that when the temperature is below 100°C, the steady state coefficient of friction is below 0.2. However, when the temperature is above 100°C but below 250°C, the coefficient of friction is between 0.4–0.5. When the temperature exceeds 250°C, the coefficient of friction increases steeply to 1.2–1.4 with a concurrent increase in temperature. The formation and presence of debris during the initial stages of the experiments causes an initial increase in the coefficient of friction, which was observed in all the experiments.

4.2. Subsurface Macrostructural and Microstructural Analyses

Figure 6 shows the macrostructures of subsurface deformation of the aluminum sample under the interaction area of the rotating tool with the base metal. At 13 MPa contact pressure and for rotation speeds of 200 rpm, 600 rpm, and 1000 rpm, there is no observable subsurface deformation. However, at the rotation speed of 1400 rpm, there is evidence of the deformed layer on both the surface and subsurface. When the contact pressure increases, the deformed layer becomes easily observable. At the higher contact pressures and rotation speeds, the deformed layer is recrystallized and is distinctly visible as seen in Fig. 6(c) for 1000 rpm, and in Fig. 6(d) for 1400 rpm, and the surface tends to take on the profile of the pin. At the higher contact pressures and tool rotation speeds, the temperature of the base material is found to be higher. Consequently, the yield pressure of the base material at the "local" level decreases, and the real contact area of the steel pin approaches an apparent contact area. For these experimental conditions, the contact pressure exceeds the yield pressure of the material at the "local" level. This is evident from the presence of a fully recrystallized region in the subsurface. Thus, as the temperature increases for a given contact pressure, the contact between the rotating tool and the base material results in conformal contact.

The representative microstructures of the subsurface that is immediately below the interaction area are shown in Fig. 7. Since the experiments were conducted at various

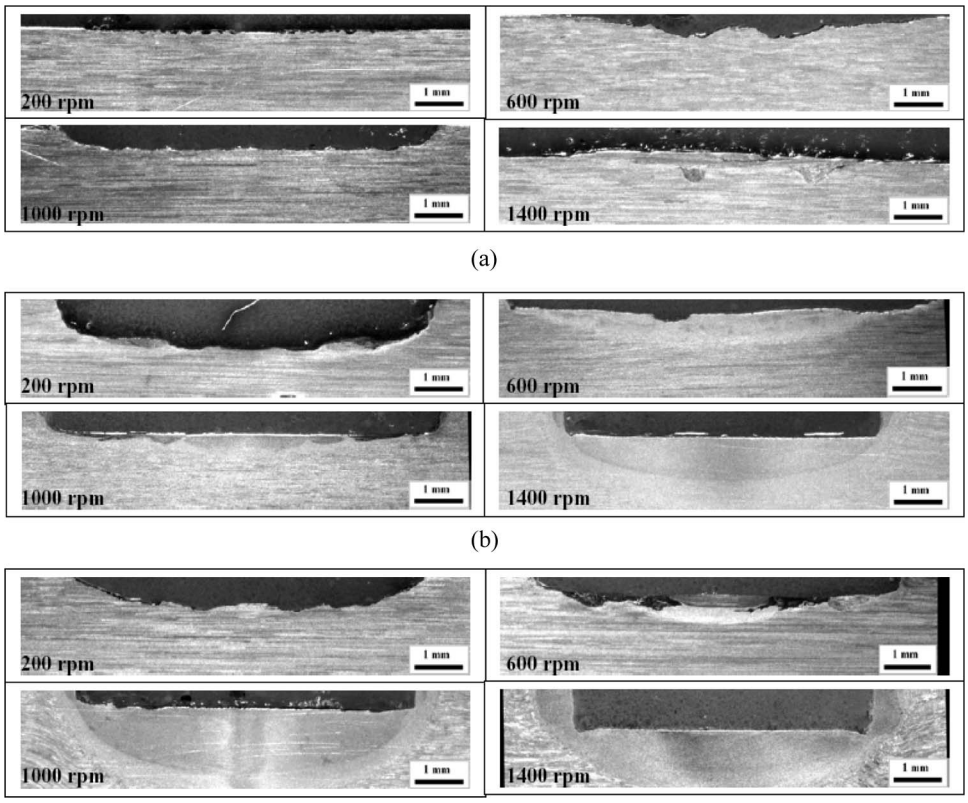

FIGURE 6.—Cross-section of the aluminium shows the macrostructure in the surface and subsurface deformation under the interacting area at contact pressures of: (a) 13 MPa; (b) 26 MPa; and (c) 39 MPa.

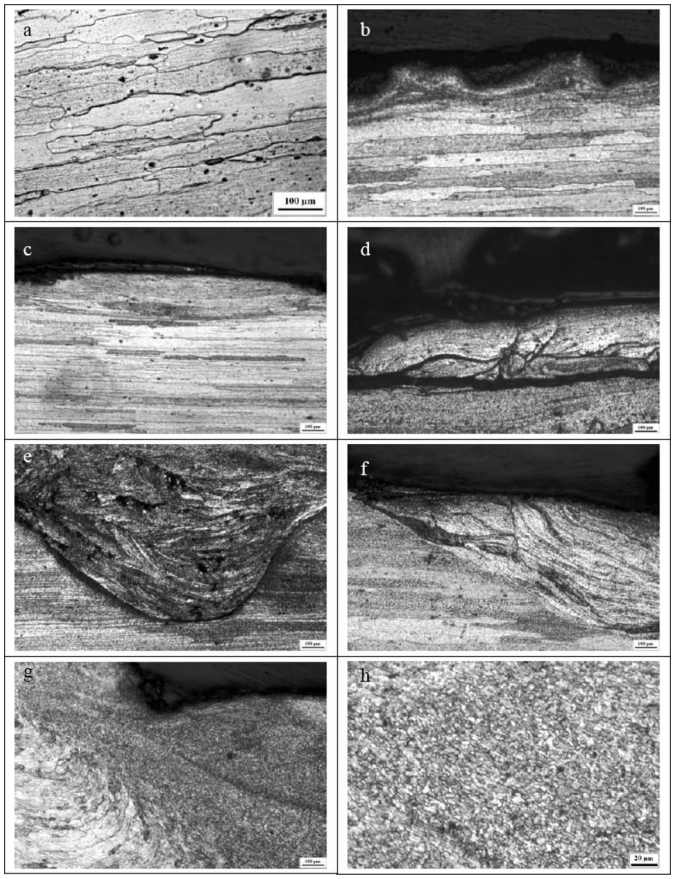

FIGURE 7.—Microstructures show various feature of surface and subsurface: (a) base metal; (b) worn surface without subsurface deformation (13 MPa and 200 rpm); (c) deformed layer (39 MPa, 200 rpm); (d) delamination of the deformed layer and debris formation (13 MPa and 1400 rpm); (e) interaction of the debris with the base metal and accumulation in the subsurface (13 MPa and 1400 rpm); (f) the severely deformed subsurface (26 MPa and 1000 rpm); (g) subsurface deformation and recrystallization; and (h) recrystallized microstructure.

contact pressures and rotation speeds, there were different wear features observed. At the higher contact pressure and rotation speeds, and resultant high temperature, the base metal was fully recrystallized in the area of interaction. The microstructure revealed that as both contact pressure and rotation speed increase, the thickness of the deformed layer increases. Upon reaching a certain temperature, the base metal tends to recrystallize. The transformation of elongated grains in the base metal to fine near-equiaxed shaped grains is shown in Fig. 7(g). Figure 7(h) shows the recrystallized microstructure in the subsurface. The observed microstructural features are quite typical of the microstructure that is observed on top of the stirred zone when the shoulder of the rotating tool is in direct contact with the base metal.

It is evident from Figs. 3–5 that, at lower temperatures, the coefficient of friction does not increase appreciably at the lower rotational speeds (200 rpm and 600 rpm). The maximum temperature in the base metal was found to be 120°C. At these two rotational speeds (200 rpm and 600 rpm), the frictional heat input to the base metal was not sufficient to increase the temperature beyond 120°C. However, at the higher contact pressures (i.e., 26 MPa and 39 MPa) and higher rotation speeds (i.e., 1000 rpm and 1400 rpm), the maximum temperature recorded was 450°C. For these rotational speeds, once the temperature reaches 250°C at the contact pressure of 26 MPa, and 200°C at the contact pressure of 39 MPa, there occurs a noticeable change in:

(a) Slope of the temperature vs. time curve;
(b) Slope of the coefficient of friction vs. time curve.

The temperature at which the slope change occurs is taken to be the critical limit at the chosen contact pressure. Once the critical limit is crossed, there occurs an increase in the friction coefficient up until 1.4 beyond which it stabilizes. Thus, the observed increase in the friction coefficient is found to be the influence of temperature, and the resultant rise in temperature is dependent on the frictional heat input.

The observed steep increase in the coefficient of friction and temperature is identified to be due to the seizure phenomenon [21–24] wherein the contact condition between the rotating tool and the workpiece material changes from the slipping mode to a sticking mode. As explained by Somi Reddy and coworker [23], the necessary conditions for seizure of the interacting surface to occur is that the real area of contact should approach the apparent area of contact at the temperature. In experiments conducted at the higher contact pressures (i.e., 26 MPa and 39 MPa) and higher rotation speeds (i.e., 1000 rpm and 1400 rpm) the real area of contact is expected to increase as the material is gradually softened due to a "local" dissolution of the strengthening precipitates coupled with an increase in process temperature as yield pressure of the material reduces. This sets off the condition that is conducive for seizure of the interacting surfaces and they seize. Further, it is noticed that the seizure phenomenon occurs at a lower temperature when the contact pressure is higher. Similar results have been reported in the published literature [25, 26]. Few research efforts have been made at analyzing the mechanism of seizure and reported for various environment conditions [27–29]. In this research study, there is evidence of the occurrence of bulk plastic deformation at the subsurface of the aluminum alloys (Figs. 6 and 7), and the thin transfer layer of aluminum is continuously formed on the rotating steel pin. Thereafter, the interaction is confined to occur only between the base metal, which is aluminum alloy, and the aluminum layer on the rotating tool.

Above the critical temperature, the friction coefficient increases steeply as a direct consequence of which the temperature increases rapidly. Thus, the friction coefficient and temperature have a synergistic influence on each other. When the frictional heat input is not sufficient to increase the temperature to the critical limit, the coefficient of friction is less than 0.5. Further, there is no evidence of recrystallization in the subsurface microstructure. Above the critical temperature, the applied contact pressure does exceed the flow stress of the material at the "local" level. Due to this, the intimacy of contact between the rotating pin and the base metal must be conformal. Since a continuous

interaction exists between the rotating pin and the base metal, at a given location, there exists minimum to no scope for the formation of an oxide layer. Consequently, the oxide-free fresh material is in continuous contact with each other. As reported by Rubenstein [26], the presence of clean surfaces, coupled with "locally" high temperature, is conducive for the occurrence of seizure. This is rationalized as being the reason for the observed steep increase in the friction coefficient above a critical temperature that was observed in this research study.

The subsurface microstructure and temperature of the base material does reveal the experimental setup to be capable of simulating the FSW condition. The "local" temperature and contact pressure in the FSW process appears to be beyond the seizure limit. Hence, the contact condition is expected to be sticking, and there does occur a transfer layer formation on the rotating steel pin. Once the sticking condition is established, the coefficient of friction is governed by shear strength of the material. In classical friction theories, the shear stress of the material is assumed to be half the yield stress of the material. However, in developing the classical theories the effect of strain rate on shear stress was not considered. In the FSW process, the strain rate is expected to be of the order of $1000\ s^{-1}$. The influence of strain rate is rationalized as being the reason for the observed discrepancy between theory and experimental findings.

5. Conclusions

Based on this experimental study and the results obtained, the following are the key findings:

1. The coefficient of friction and temperature do have a synergic influence on each other.
2. The coefficient of friction in the FSW condition was found to be as high as 1.2–1.4 at 400°C to 450°C.
3. The critical temperature seizure observed is 250°C for a contact pressure of 26 MPa and 200°C for a contact pressure of 39 MPa. The critical temperature decreases with increasing contact pressure.
4. The temperature and contact pressure in the FSW process appears to be beyond the seizure limit.

References

1. Thomas, W.M.; Nicholas, E.D.; Needham, J.C.; Murch, M.G.; Templesmith, P.; Dawes, C.J.G.B. Patent Application No. 9125978.8 (December, 1991).
2. Dawes, C.; Thomas, W. TWI Bulletin, November–December, 1995; 124.
3. Thomas, W.M. Friction Stir Butt Welding; International Patent Application No PCT GB 92 Patent Application No. 9125978.8, 1991.0R.
4. Dawes, C.J. Proceeding of the Sixth International Symposium, JWS: Nagoya, Jaspan, 1996.
5. Threadgill, P.L. *Friction Stir Welds in Aluminum Alloys*; TWI Bulletin: United Kingdom, 1997.
6. Thomas, W.M.; Nicholas, E.D. Proceedings of the Third World Congress on Aluminum, Limassol, Cyprus, 1997.
7. Mahoney, M.W. Welding and Joining 1997.
8. Schneider, J.; Beshears, R.; Nunes, Jr., A.C. Materials Science and Engineering A **2006**, *435–436*, 297–304.
9. Frigaard, O.; Grong, O.; Midling, O.T. Metallurgical and Materials Transactions A **2001**, *32*, 1189–1200.
10. Mishra, R.S.; Ma, Z.Y. Materials Science and Engineering **2005**, *50*, 1–78.
11. Song, M.; Kovacevic, R. International Journal of Machine Tools and Manufacture **2003**, *43*, 605–615.
12. Chen, C.M.; Kovacevic, R. International Journal of Machine Tools and Manufacture **2003**, *43*, 1319–1326.
13. Schmidt, H.B.; Huttel, J.H. Scripta Materialia **2008**, *58*, 332–337.
14. Colligan, K.J.; Mishra, R.S. Scripta Materialia **2008**, *58*, 327–331.
15. Beynon, J.H. Tribology International **1998**, *31*, 73–77.
16. Chen, Z.; Thomson, P.F. Wear **1996**, *201*, 221–232.
17. Duffin, F.D.; Bahrani, A.S. Wear **1973**, *26*, 53–74.
18. Reid, J.V.; Schey, J.A. Adhesion of copper alloys. Wear **1985**, *104*, 1–20.
19. Starke, E.A. Jr. In *Fatigue and Microstructure*; Meshii, M., Ed.; American Society for Metals (ASM) Metals Park: Ohio, USA, 1979.
20. Nicolas, M.; Deschamps, A. Acta Materialia **2003**, *51*, 6077–6094.
21. Farhat, Z.N.; Ding, Y.; Northwood, D.O.; Alpas, A.T. Materials Science and Engineering A **1996**, *206*, 302–313.
22. Peng, Z.; Kessissoglou, N. Wear **2003**, *255*, 1221–1232.
23. Somi Reddy, A.; Pramila Bai, B.N.; Murthy, K.S.S.; Biswas, S.K. Wear **1995**, *181–183*, 658–667.
24. Mosleh, M.; Saka, N.; Suh, N.P. A mechanism of high friction in dry sliding bearings. Wear **2002**, *252*, 1–8.
25. Wang, Q. Seizure failure of journal-bearing conformal contacts. Wear **1997**, *210*, 8–16.
26. Rubenstein, C. Wear **1958/1959**, *2*, 85–96.
27. Chandrasekaran, M.; Batchelor, A.W.; Loh, N.L. Tribology International **2002**, *35*, 297–308.
28. Krithivasan, R.; Khonsari, M.M. Transactions of the ASME. Journal of Tribology **2003**, *125*, 833–841.
29. Pal, A.K. Wear **1973**, *26*, 261–272.